Laser & Photonics Reviews

LASER & PHOTONICS REVIEWS

www.lpr-journal.org

RESEARCH ARTICLE

Greatly Enhanced Photoluminescence From a $Si/WS_2/Si_3N_4/Ag$ Nanocavity by Exploiting the Electron Transfer Induced by Femtosecond Laser Pulses

Shimei Liu[1] | Zhuo Wang[2] | Shulei Li[3] | Yuheng Mao[2] | Mingcheng Panmai[4] | Jinhao Zhou[1] | Dong Yan[1] | Yongyao Li[1] | Dongxu Zhao[1] | Sheng Lan[2]

[1]Guangdong-HongKong-Macao Joint Laboratory for Intelligent Micro-Nano Optoelectronic Technology, School of Physics and Optoelectronic Engineering, Foshan University, Foshan, P. R. China | [2]Guangdong Provincial Key Laboratory of Nanophotonic Functional Materials and Devices, School of Optoelectronic Science and Engineering, South China Normal University, Guangzhou, P. R. China | [3]School of Physics and Optoelectronic Engineering, Guangdong Polytechnic Normal University, Guangzhou, P. R. China | [4]Division of Physics and Applied Physics, School of Physical and Mathematical Sciences, Nanyang Technological University, Singapore

Correspondence: Dongxu Zhao (zhaodx@fosu.edu.cn) | Sheng Lan (slan@scnu.edu.cn)

Received: 10 February 2026 | **Revised:** 24 April 2026 | **Accepted:** 2 May 2026

Keywords: electron transfer | nanocavity | photoluminescence | transition metal dichalcogenide | two-photon absorption

ABSTRACT

Monolayer transition metal dichalcogenides hold great potential for quantum photonic devices owing to their unique physical properties. However, the atomically thin nature of these materials fundamentally limits their light absorption, which in turn constrains the efficiency and intensity of exciton emission. Here, we resonantly excited a WS_2 monolayer embedded in a $Si/Si_3N_4/Ag$ nanocavity composed of a silicon (Si) nanoparticle and a Si_3N_4/Ag heterostructure by using femtosecond laser pulses, strongly enhancing two-photon absorption in the Si nanoparticle. The generated electrons transfer to the WS_2 monolayer, effectively compensating for its weak optical absorption. We observed a significantly enhanced photoluminescence (PL) intensity of the $Si/WS_2/Si_3N_4/Ag$ nanocavity under femtosecond laser excitation compared to continuous-wave laser excitation. Simultaneous enhancement of the excitation rate, emission intensity and emission directionality induced by double resonances further boosts the PL intensity in the WS_2 monolayer. The weak coupling between the exciton and magnetic dipole resonance additionally enhances the PL intensity and leads to a redshift in the PL spectrum. We obtain a PL enhancement factor as large as ≈ 13729 in the nanocavity at low laser power. Our findings suggest that the manipulation of carrier dynamics in hybrid nanocavities offers a promising strategy for the development of novel light-emitting devices.

1 | Introduction

Monolayer transition metal dichalcogenides (TMDCs), such as tungsten diselenide (WSe_2) and tungsten disulfide (WS_2), have been the focus of attention as promising materials for light-matter interactions and optoelectronic devices [1–3]. In general, a monolayer TMDC is a semiconductor with a direct bandgap [4–8], implying potential applications in light-emitting devices. In addition, monolayer TMDCs also hold great potential for quantum photonic devices, as their large exciton binding energies (hundreds of meV) support deterministic single-photon emission from defect-bound and strain-localized exciton states at cryogenic temperatures, with emission wavelength, polarization, and charge state tunable via strain engineering and gate voltage [9–11]. However, due to their ultrathin nature, the weak light absorption in monolayer TMDCs, particularly at wavelengths away from

exciton resonances, limits their single- and two-photon luminescence, which hinders the development of practical devices [4]. Various strategies have been proposed to overcome this issue, including the use of strain [12–14] and carrier doping [15], control of the surrounding dielectric environment [16] and the local photonic environment [17, 18]. Additionally, the strategic selection of TMDCs allows for the creation of Type-I van der Waals heterostructures, where the confinement of both electrons and holes in the same layer significantly enhances photoluminescence (PL) [19]. In previous works, it has been reported that the PL enhancement can also be achieved by the nonradiative energy transfer from the material with a higher work function to that with a lower one [20–22]. Recently, it has been demonstrated that plasmon-enhanced hot-electron transfer can boost the PL intensity of the monolayer TMDC [23]. Moreover, non-uniform strain creates local potential wells in monolayer TMDCs, leading to the enhancement of PL intensity [12, 13, 24]. Importantly, PL enhancement can be achieved through weak coupling between plasmon and exciton with the PL spectrum dominated by the emission from the lower plexciton branch [18, 25, 26]. Therefore, it is expected that the enhanced PL can also be achieved by exploiting the electron transfer at the interface between dielectric nanoparticles and monolayer TMDCs.

Silicon (Si) nanoparticles with appropriate sizes can support Mie resonances and function as artificial atoms for metamaterials operating at optical frequencies [27–29]. These optical resonances enhance multi-photon absorption by increasing the local density of states. Such enhancement is particularly pronounced in all-dielectric materials like Si, where, under conditions of resonance excitation, the resonance-enhanced electric field is strongly localized within the Si nanoparticle. This localization directly contributes to the enhancement of two-photon absorption (2PA) and three-photon absorption [30]. Single Si nanoparticles exhibit highly efficient harmonic generation and hot electron luminescence when their Mie resonances, particularly the magnetic dipole (MD) resonance, are excited [31, 32]. More importantly, injecting high-density carriers can significantly alter the carrier dynamics within the Si nanoparticle [33]. In addition, it has been reported that a $Si/Si_3N_4/Ag$ nanocavity enables a luminescence burst at a lower excitation energy ($\approx$ 20.5 pJ) compared to that of a Si nanoparticle placed on a silica (SiO_2) substrate ($\approx$ 51.3 pJ) [34]. Furthermore, since the conduction band energy of the Si at Γ point is higher than that of the WS_2 monolayer at K point, efficient electron transfer from the Si to the WS_2 monolayer can be readily achieved. Therefore, the enhanced 2PA in the Si nanoparticle on the Si_3N_4/Ag heterostructure offers a strategy to overcome the weak absorption in the WS_2 monolayer by utilizing electron transfer from the Si nanoparticle to the WS_2 monolayer.

In recent years, a variety of optical nanocavities have been successfully employed to achieve the PL enhancement of monolayer TMDCs, including metallic film-coupled metallic nanocubes or Si nanospheres [18, 26, 35]. Basically, the PL enhancement of monolayer TMDCs relies mainly on improving the excitation rate, quantum efficiency, and emission directionality [36, 37]. The enhancement in the quantum efficiency is determined by the Purcell factor, which is proportional to Q/V, where Q and V represent the quality factor and the optical mode volume, respectively [36, 38]. In order to achieve maximum PL enhancement in monolayer TMDCs, one can use a suitably designed dielectric nanocavity that supports multiple resonances with diverse electromagnetic field distributions, allowing for the realization of simultaneous enhancement at the excitation and emission wavelengths [38]. Moreover, effective control over the emission properties is of crucial importance for realizing unique functionalities of emitters. By carefully selecting the resonant mode, a dielectric nanoantenna can be used to efficiently modulate the far-field radiation pattern, leading to the directional emission of the PL [39–41]. Therefore, dielectric nanocavities not only promote electron transfer but also provide simultaneous enhancement in excitation, emission, and directionality.

In this article, we propose the use of a $Si/Si_3N_4/Ag$ nanocavity excited by femtosecond (fs) laser pulses to achieve PL enhancement in an embedded WS_2 monolayer. Compared to the single-photon absorption (1PA) spectrum calculated for the WS_2 monolayer within the nanocavity, the significantly enhanced 2PA in the Si nanoparticle suggests the efficient electron transfer from the Si nanoparticle to the WS_2 monolayer. Furthermore, the enhanced in-plane electric field in the nanocavity at both the excitation and emission wavelengths can simultaneously boost the excitation and emission of excitons in the WS_2 monolayer. We experimentally examined the PL spectra of $Si/WS_2/Si_3N_4/Ag$ nanocavities composed of Si nanoparticles with different diameters under both fs and continuous-wave (CW) laser excitation. The PL enhancement observed in the $Si/WS_2/Si_3N_4/Ag$ nanocavity under fs excitation was significantly greater than that under CW excitation. We demonstrated that a significant PL enhancement factor (EF) $\approx$ 13729 can be obtained by the combined effects of electron transfer, weak coupling and double Mie-type resonances.

2 | Results and Discussion

2.1 | Physical Mechanism for the Enhanced PL Emission from a $Si/WS_2/Si_3N_4/Ag$ Nanocavity Excited by fs Laser Pulses

Figure 1a shows the schematic of a $Si/WS_2/Si_3N_4/Ag$ nanocavity composed of a Si nanoparticle, an embedded WS_2 monolayer, a 90 nm-thick Si_3N_4 layer and a 50 nm-thick Ag film deposited on a SiO_2 substrate. Figure 1b illustrates energy band diagram and carrier dynamics in the $Si/WS_2/Si_3N_4/Ag$ nanocavity excited by fs laser pulses. The diagram reveals that a potential well forms in the WS_2 monolayer, while the Si_3N_4 layer with a large bandgap serves as a potential barrier to confine electrons. In this case, electron–hole pairs are simultaneously generated in the conduction and valence bands of the WS_2 monolayer following 1PA in the WS_2 monolayer upon excitation of fs laser pulses. Since most excitons in the WS_2 monolayer are horizontally oriented, the 1PA is proportional to the second power of the in-plane electric field inside the embedded WS_2 monolayer (i.e., $I \propto (1/V) \int_{WS_2} (|E_{xy}|/|E_0|)^2 dV$). Since the 2PA is proportional to the fourth power of the electric field inside the Si nanoparticle (i.e., $I^2 \propto (1/V) \int_{Si} (|E|/|E_0|)^4 dV$), the 2PA in the Si nanoparticle can be significantly enhanced when the maximum electric field is achieved. Therefore, high-density electron–hole pairs can be generated in the Si nanoparticle under

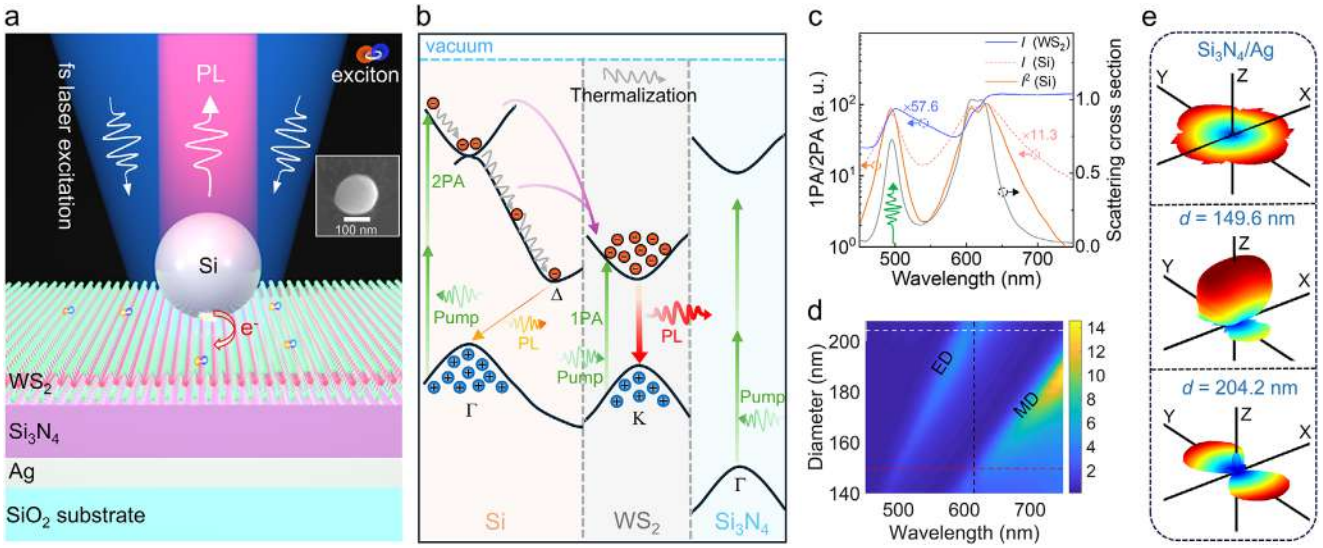

FIGURE 1 | Physical mechanism for the enhanced PL emission from a Si/WS_2/Si_3N_4/Ag nanocavity excited by fs laser pulses. (a) Schematic showing PL enhancement (red light) in a WS_2 monolayer embedded in a Si/Si_3N_4/Ag nanocavity upon the excitation of a fs laser (blue light). Scanning electron microscopy image of a Si nanoparticle shown in the inset. (b) Energy band diagram and carrier dynamics in the Si/WS_2/Si_3N_4/Ag nanocavity excited by fs laser pulses, illustrating the PL enhancement mechanism via electron transfer from the Si nanoparticle to the WS_2 monolayer. (c) Calculated spectra of a Si/WS_2/Si_3N_4/Ag nanocavity (d = 149.6 nm): scattering spectrum (gray solid line), 1PA (pink dashed curve) and 2PA (orange solid curve) spectra of the Si nanoparticle, and 1PA spectrum (blue solid curve) of the embedded WS_2 monolayer. (d) In-plane electric field enhancement ($(1/V)\int_{WS_2}(|E_{xy}(\lambda)|/|E_0|)^2 dV$) calculated for Si/$WS_2$/$Si_3N_4$/Ag nanocavities composed of Si nanoparticles with different diameters. The exciton resonance (615 nm) of the WS_2 monolayer is denoted by a vertical black line. Two nanocavities with d = 149.6 nm (red dashed line) and d = 204.2 nm (white dashed line) are highlighted by horizontal lines. (e) 3D radiation patterns calculated for a Si_3N_4/Ag planar structure and two Si/Si_3N_4/Ag nanocavities (d = 149.6 and d = 204.2 nm).

resonant excitation. As shown in Figure 1b, under 515 nm fs laser excitation, abundant low-energy electrons in the valence band can be directly excited to high-energy states in the conduction band [42]. Subsequently, these high-energy hot electrons undergo rapid thermalization through electron–electron and electron–phonon scattering, relaxing to the Γ valley of the conduction band. Then, the hot electrons undergo rapid relaxation from the Γ valley to the Δ valley via phonon emission, followed by radiative recombination. Importantly, during the relaxation of electrons from high-energy states to the Δ valley, a portion of the hot electrons can efficiently transfer from the Si nanoparticle to the conduction band of the WS_2 monolayer. The accumulated carriers in the WS_2 monolayer then recombine radiatively, giving rise to the enhanced PL intensity. In Figure 1c, we present the calculated scattering spectrum of a Si/WS_2/Si_3N_4/Ag nanocavity, the 1PA/2PA spectra for a Si nanoparticle in the nanocavity, and the 1PA spectrum for an embedded WS_2 monolayer. The peaks observed in the scattering spectrum correspond to MD and electric dipole (ED) resonances with relatively narrow linewidths, indicating that the Q factors of the ED and MD resonances are improved by using the Si_3N_4/Ag heterostructure (see Note S1) [34]. A shallow dip can be observed in the scattering spectrum, which originates from the weak coupling between the exciton and MD resonance. Additionally, one can observe the enhanced optical absorption at the MD and ED resonances. The weak 1PA (pink dashed curve) suggests that the low-density carriers are generated in the Si nanoparticle upon excitation by a CW laser. In contrast, the 2PA in the Si nanoparticle is remarkably enhanced exhibiting an enhancement factor of ≈ 11.3 relative to the 1PA in the Si nanoparticle. Consequently, a high density of carriers is generated in the conduction and valence bands of the Si nanoparticle when the nanocavity is resonantly excited by a fs laser. Furthermore, the 1PA in the WS_2 monolayer embedded in the nanocavity is ≈ 21.4 times stronger than that on the Si_3N_4/Ag heterostructure (see Note S2).

The localized electric field induced by the nanocavity is expected to simultaneously enhance the excitation and emission processes in the WS_2 monolayer. Since excitons are primarily affected by the in-plane electric field (E_{xy}) of the nanocavity, the in-plane electric field magnitudes at the excitation and emission wavelengths determine the excitation enhancement and emission rate enhancement (i.e., Purcell factor), respectively. Therefore, we first examined the wavelength-dependent in-plane electric field enhancement ($(1/V)\int_{WS_2}(|E_{xy}(\lambda)|/|E_0|)^2 dV$) for Si/$WS_2$/$Si_3N_4$/Ag nanocavities composed of Si nanoparticles with different diameters (d), as shown in Figure 1d (see also Note S3). One can identify the enhanced electric field induced by the ED and MD resonances. By varying the diameter of the nanoparticle, the ED and MD resonances can be tuned to match the excitation and emission wavelengths (red dashed line), thereby simultaneously enhancing the excitation and emission processes. Furthermore, for the larger nanocavity (white dashed line), the ED resonance with the enhanced electric field is shifted to the exciton resonance (black dashed line). Apart from enhancing excitation and emission processes, the Si/Si_3N_4/Ag nanocavity is also employed to engineer the emission directionality of excitons. We further simulated the three-dimensional (3D) radiation patterns of a dipole source located at the Si_3N_4/Ag heterostructure

and Si/Si_3N_4/Ag nanocavities, as shown in Figure 1e. It is noticed that the radiation pattern of the dipole source is dramatically reshaped and the backward radiation intensity is significantly enhanced in the presence of the Si nanoparticle, leading to the enhancement of the collected PL signal in experiments. Furthermore, the backward radiation intensity induced by the MD resonance is stronger compared to that induced by the ED resonance (see also Figure S4). Moreover, the Purcell factor, obtained by integrating the radiation intensity of a dipole emitter located at the nanocavity (d = 149.6 nm), is derived to be ≈ 3 (see also Note S4), which is consistent with values reported in the literature with similar structures [43, 44]. Meanwhile, using an oil-immersion objective with a numerical aperture (NA) of 1.3 (corresponding to a collection half-angle of ≈ 60°), the detected PL *EF* due to improved collection efficiency reaches as high as ≈ 13. Therefore, it is expected that enhanced PL intensity from the WS_2 monolayer can be achieved by utilizing the MD and ED resonances supported by the Si/Si_3N_4/Ag nanocavity.

2.2 | Enhanced PL Intensity from Si/WS_2/Si_3N_4/Ag Nanocavities Under the Excitation of fs Laser Pulses

Figure 2a,b show bright- and dark-field images of a WS_2 monolayer formed on a Si_3N_4/Ag heterostructure. It was obtained by transferring a WS_2 monolayer grown by chemical vapor deposition (CVD) onto the Si_3N_4/Ag heterostructure via a wet-transfer method (see Methods for details). In Figure 2b, one can identify two Si nanoparticles (enclosed by dashed circles) located on the WS_2/Si_3N_4/Ag planar structure, which exhibit orange scattering light. Figure 2c presents the backward scattering spectra measured for these two Si/WS_2/Si_3N_4/Ag nanocavities (pink solid curves), alongside the calculated scattering spectra for comparison (purple dashed curves). In both cases, the MD and ED resonances supported by the nanocavities manifest as scattering peaks. The resonant wavelengths of the MD (λ_{MD}) are 607 and 630 nm, respectively, which are close to the exciton resonance of the WS_2 monolayer. In addition, the resonant peak (MD) in the scattering spectrum of nanocavity A exhibits an asymmetric lineshape with a small shoulder on the long-wavelength side, rather than a distinct dip (see Figure S5b), which originates from the MD resonance being slightly detuned from the exciton resonance. It indicates weak coupling between the MD resonance and the exciton (see also Note S5). The measured MD resonant wavelengths are essentially consistent with the simulated results, whereas a slight discrepancy in the ED resonant wavelengths exists between the experimental and simulated spectra, which arises from the non-spherical morphology of Si nanoparticles fabricated via fs laser ablation. In Figure 2d, we present the PL spectra measured for these two Si/WS_2/Si_3N_4/Ag nanocavities under the excitation of a 488 nm CW laser (see also Note S6). For reference, the PL spectrum from the adjacent WS_2/Si_3N_4/Ag planar structure is also shown in each case. The PL intensities of both nanocavities are enhanced, which is further corroborated by the brighter PL emission observed in the corresponding charge coupled device (CCD) images. In this case, the radiative recombination of excitons is accelerated by the MD resonance, resulting in an enhancement of the emission. This enhancement is characterized by using the relative intensity ((I-I_0)/I_0), where I and I_0 are the PL intensities of the Si/WS_2/Si_3N_4/Ag nanocavity and the WS_2/Si_3N_4/Ag planar structure, respectively. A relative PL intensity of ≈ 5.6 can be obtained for nanocavity A, which is slightly higher than that of nanocavity B. Since the exciton resonances in both Si/WS_2/Si_3N_4/Ag nanocavities are slightly detuned from the corresponding MD resonances of the nanocavities, this modest enhancement may be attributed to its higher excitation rate (see Figure 2c). Furthermore, a pronounced redshift is observed in the PL spectra, with the maximum PL peak redshift of ≈ 14.2 nm. This redshift is mainly attributed to emission from the lower plexciton, which originates from weak coupling between the exciton and MD resonance (see also Note S5) [25]. The wavelength difference (≈ 10 nm) between the lower plexciton and the exciton (see Figure S5a) is in close agreement with the magnitude of the experimentally observed redshift. Figure 2e presents the PL spectra measured for these two Si/WS_2/Si_3N_4/Ag nanocavities and the adjacent WS_2/Si_3N_4/Ag planar structure under the excitation of a 515 nm fs laser. The maximum redshift reaches ≈ 11.6 nm, which is slightly smaller than that under the CW laser excitation, likely owing to the reduced thermal effects. Notably, the PL intensities of the Si/WS_2/Si_3N_4/Ag nanocavities are significantly enhanced, with nanocavity B exhibiting a relative PL intensity as high as ≈ 53. This value is an order of magnitude higher than that under 488 nm CW laser excitation. Due to the weak 1PA observed in the Si nanoparticle under the CW laser excitation, this process can only generate low-density electrons at the lower-energy Δ point, preventing electron transfer from the Si nanoparticle to the WS_2 monolayer. In contrast, the mechanism underlying the significant PL enhancement is the electron transfer from the Γ point of the Si nanoparticle to the conduction band of the WS_2 monolayer, driven by the generation of high-density carriers in the Si nanoparticle excited by fs laser pulses. Ideally, a fair comparison between the two excitation schemes requires matching their excitation wavelengths. However, the optical parametric oscillator, although providing tunable output, has a minimum achievable wavelength limited to 503 nm, thus preventing matching with the fixed wavelength (488 nm) of the CW laser. Thus, the significant PL enhancement in these two nanocavities under fs laser excitation might be attributed to resonance between the 515 nm laser wavelength and the ED resonance (see Note S7). To verify this hypothesis, we investigated nanocavities with modes resonant at 488 nm but detuned from 515 nm (see Note S7). Despite this detuning, these nanocavities still exhibit a larger PL enhancement under non-resonant fs laser excitation than under resonant CW laser excitation at 488 nm. The relative PL intensity of nanocavity B (≈ 53) is greater than that of nanocavity A (≈ 30), which stems from the amplified emission due to resonance between the exciton (631 nm) and the MD of nanocavity B.

In addition, since the sizes of the hot spot (approximately equal to the diameter of the nanocavity; see Note S3) and the region of the electron transfer are much smaller than those of the laser spot (≈ 1 μm), it is expected that the actual *EF* of the PL intensity will be much greater than that observed in the experiment (see also Note S8). Basically, the *EF* of PL intensity in the nanocavity can be calculated by using the following formula:

$$EF = \frac{\int_{S_0} I(x,y)\,dS}{\int_{S_1} I(x,y)\,dS} \frac{I - I_0}{I_0} \quad (1)$$

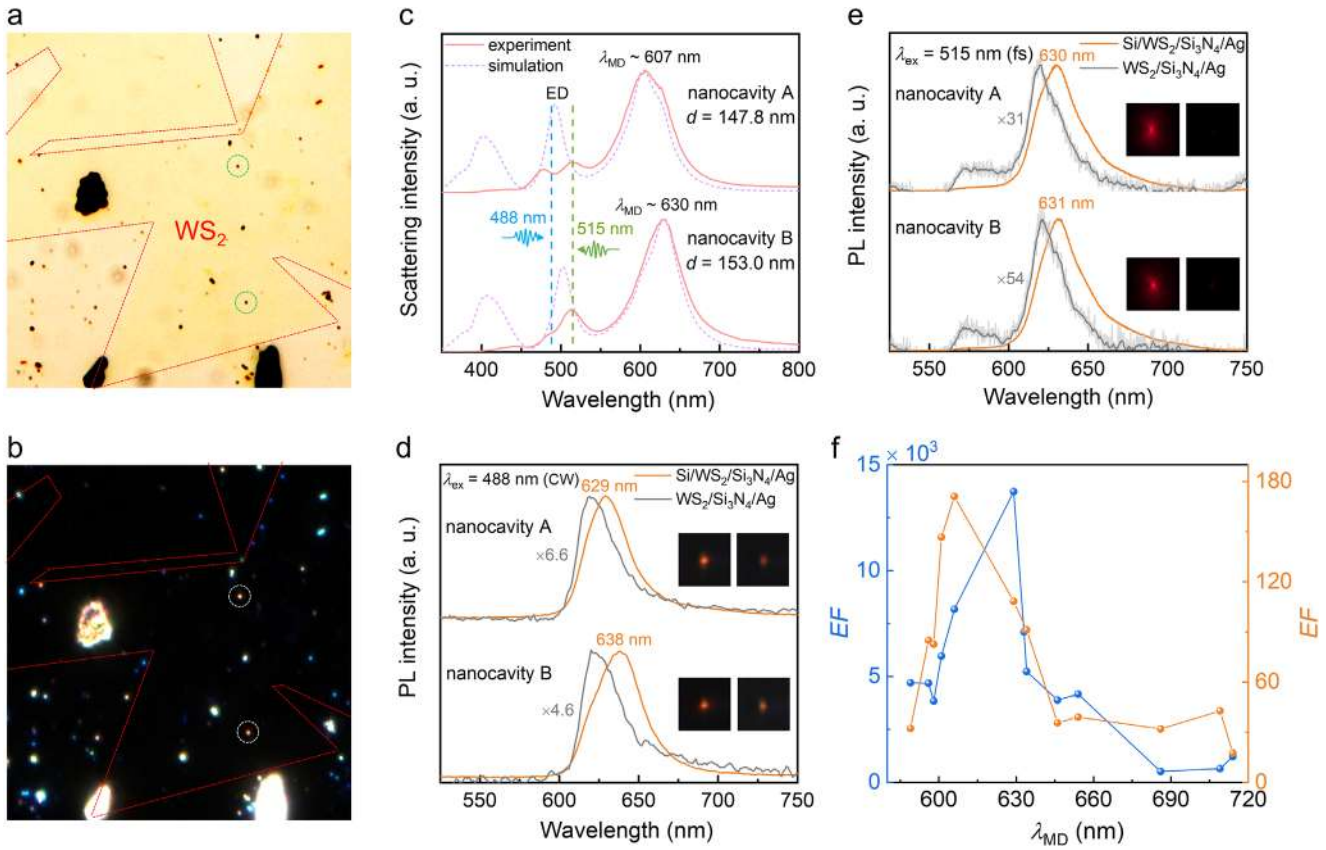

FIGURE 2 | Enhanced PL intensity from Si/WS_2/Si_3N_4/Ag nanocavities under the excitation of fs laser pulses. (a, b) bright- and dark-field optical microscopy images of a WS_2/Si_3N_4/Ag planar structure and Si/WS_2/Si_3N_4/Ag nanocavities. Two Si nanoparticles used to construct the nanocavities are marked with dashed circles. (c) Backward scattering spectra (pink solid curves) measured for these two Si/WS_2/Si_3N_4/Ag nanocavities. Backward scattering spectra (purple dashed curves) calculated for two nanocavities with d = 147.8 nm and d = 153.0 nm, respectively. (d) PL spectra measured for aforementioned two nanocavities (orange curves) under the excitation of a 488 nm CW laser. PL spectra of the WS_2/Si_3N_4/Ag planar structures (gray curves) are also provided for comparison. The CCD images of the corresponding PL emission are shown in the insets. (e) PL spectra measured for these two nanocavities (orange curves) under the excitation of a 515 nm fs laser. PL spectra of the WS_2/Si_3N_4/Ag planar structures (gray curves) are also provided for comparison. The CCD images of the corresponding PL emission are shown in the insets. (f) Dependence of the PL *EF* on the MD resonant wavelength (λ_{MD}) of the nanocavities under the excitation of the 488 nm CW laser (orange curve) and the 515 nm fs laser (blue curve).

where $I(x, y)$ is the spatial intensity profile of the laser beam, S_0 denotes the area corresponding to full width at half maximum of $I(x, y)$, and S_1 represents the area of the hot spot (CW laser excitation) or the region of electron transfer (fs laser excitation). Therefore, the PL *EF*s for nanocavity B under the CW and fs laser excitation are found to be ≈ 108 and ≈ 13729, respectively.

In order to demonstrate the PL intensity enhancement induced by the Purcell effect, we present the dependence of the PL *EF* on the resonant wavelength of the MD supported by the Si/WS_2/Si_3N_4/Ag nanocavities, as shown in Figure 2f (see also Note S9). For the nanocavities excited by a 488 nm CW laser, the PL *EF* first increases and then decreases with the increase of λ_{MD}. It reaches a maximum when the MD resonance is tuned near the exciton resonance (nanocavity A) due to weak coupling. Thus, the PL *EF* can be manipulated by tuning λ_{MD} via adjusting the diameter of the Si nanoparticles used to construct the nanocavities. In addition, under the excitation of a 515 nm fs laser, the PL *EF* shows a similar dependence on λ_{MD}, with a maximum achieved at 630 nm (nanocavity B). Moreover, the PL *EF*s of nanocavities excited by the fs laser are consistently and significantly higher than those excited by the CW laser in all cases. Therefore, a significant PL enhancement can be achieved by tuning the MD resonance to match the exciton resonance under the excitation of the fs laser.

2.3 | Wavelength-Dependent PL Intensity of the Si/WS_2/Si_3N_4/Ag Nanocavities

Since the laser wavelength affects the 2PA in the Si nanoparticle and the 1PA in the WS_2 monolayer, we further investigated the effect of laser wavelength on the PL enhancement in the Si/WS_2/Si_3N_4/Ag nanocavity. Since the electric field enhancement induced by ED resonance determines the excitation enhancement, we first examined the electric field distributions $|E_{xy}|/|E_0|$ in the XY plane and $|E|/|E_0|$ in the XZ plane for nanocavity B at the ED resonant wavelength, as shown in Figure 3a. In two cases, the nanocavities were excited by using a plane wave polarized along the x direction. One can see that the electric field enhancement in the Si nanoparticle is stronger than that in the WS_2 monolayer. In Figure 3b, we also examined the 2PA spectra of Si nanoparticles and the 1PA spectra of WS_2 monolayers

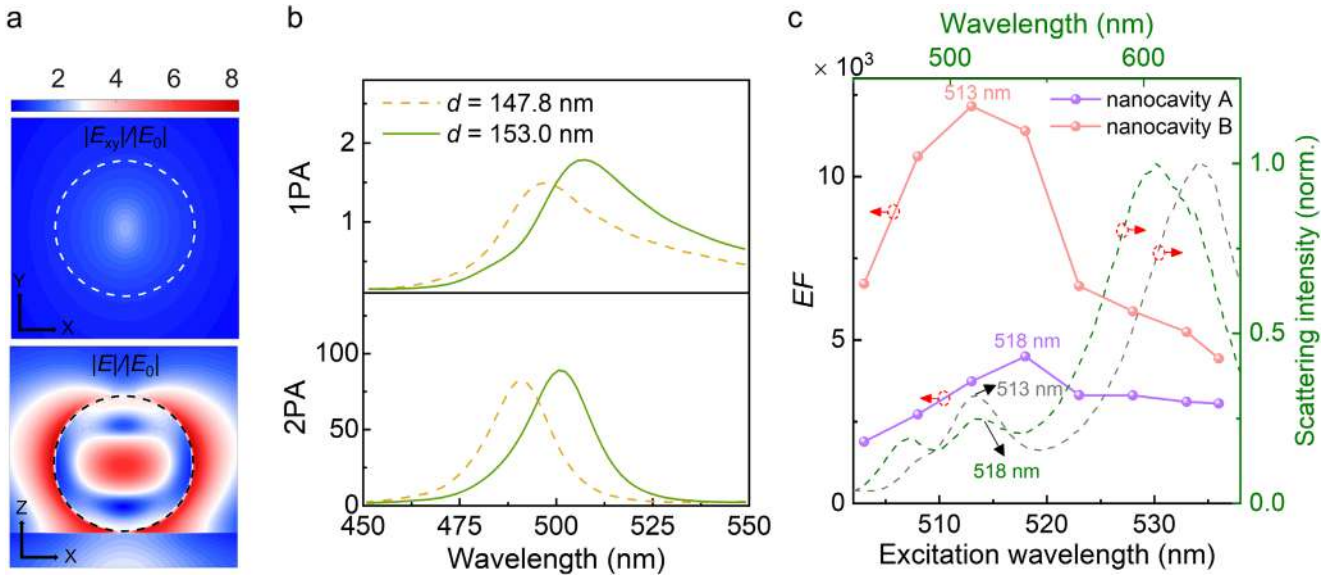

FIGURE 3 | Wavelength-dependent PL intensity of the Si/WS_2/Si_3N_4/Ag nanocavities. (a) In-plane electric field distribution ($|E_{xy}|/|E_0|$) within the WS_2 monolayer in the XY plane and electric field distribution ($|E|/|E_0|$) in the XZ plane, calculated for a Si/WS_2/Si_3N_4/Ag nanocavity with $d = 153.0$ nm (nanocavity B) at the ED resonance. (b) 2PA spectra of the Si nanoparticles and 1PA spectra of the WS_2 monolayers, calculated for two Si/WS_2/Si_3N_4/Ag nanocavities with $d = 147.8$ nm (nanocavity A) and $d = 153.0$ nm (nanocavity B), respectively. (c) PL *EF* of the two nanocavities as a function of the fs laser excitation wavelength at a laser power of $P = 30$ μW. Backward scattering spectra of nanocavity A (green dashed curve) and nanocavity B (gray dashed curve) are also provided for comparison.

for two Si/WS_2/Si_3N_4/Ag nanocavities with $d = 147.8$ nm and $d = 153.0$ nm, respectively. It can be seen that the 1PA and 2PA in nanocavity B are stronger than those in nanocavity A. The peak of the 2PA spectrum lies near the ED resonance (see also the purple curves in Figure 2c), indicating that matching the laser wavelength to the ED resonance can yield a greater PL enhancement. Therefore, we carried out PL measurements for these two Si/WS_2/Si_3N_4/Ag nanocavities by using excitation wavelengths (λ_{ex}) ranging from 503 to 536 nm and derived the dependence of the PL *EF* on the fs laser wavelength, as shown in Figure 3c (see also Note S9). In nanocavity A, we observe a rapid increase in the PL *EF* from ≈1889 to ≈ 4496 as the excitation wavelength increases to 518 nm. Beyond this wavelength, it quickly decreases to ≈ 3059 at $\lambda_{ex} = 536$ nm. In nanocavity B, the PL *EF* also increases sharply from ≈ 6719 to a maximum of ≈ 12154 at $\lambda_{ex} = 513$ nm, before decreasing to ≈ 4431 at $\lambda_{ex} = 536$ nm. It is noticed that the excitation wavelengths corresponding to the maximum PL *EF*s are close to the resonant wavelengths of the ED supported by both nanocavities (see the dashed curves). The PL *EF* of the nanocavity B under resonant excitation is 2.7-fold higher than that under off-resonant excitation. Notably, the PL *EF* achieved under fs laser excitation is up to 127 times that obtained under CW laser excitation (see Figure 2f), indicating that the significant PL enhancement in the Si/WS_2/Si_3N_4/Ag nanocavity is mainly attributed to the use of fs laser excitation. Furthermore, the PL *EF* of nanocavity B is larger compared to that of nanocavity A due to the enhanced 2PA and 1PA in nanocavity B. Therefore, a significant PL enhancement can be realized through the combination of electron transfer induced by the enhanced 2PA, excitation enhancement and emission rate enhancement enabled by the ED and MD resonances supported by the Si/WS_2/Si_3N_4/Ag nanocavity.

2.4 | Power-Dependent PL Intensity of a Si/WS_2/Si_3N_4/Ag Nanocavity

As demonstrated above, the PL intensity of the Si/WS_2/Si_3N_4/Ag nanocavity can be manipulated by tuning the excitation wavelength and shifting its MD resonance via adjusting the diameter of the Si nanoparticle. Therefore, the PL intensity is correlated with the energy difference between the MD resonance and the exciton resonance. For dynamic control, beyond varying the excitation wavelength, it is desirable to achieve PL manipulation by altering other excitation conditions. Previous studies have shown that increasing laser power can redshift the exciton resonance via the thermal effect [45], offering an opportunity to dynamically modify the energy detuning between the MD resonance and the exciton resonance, and thus manipulate the PL intensity of the nanocavity [35]. In Figure 4a, we present the PL spectra of nanocavity B measured with fs laser power ranging from 6 to 48 μW. As the laser power increases, the PL intensity rises and the PL peak redshifts from 622 to 632 nm, causing exciton resonance to approach and then cross the MD resonance (≈ 630 nm). As shown in Figure 4b,c, the dependence of the integrated PL intensity for the WS_2/Si_3N_4/Ag planar structure and nanocavity B on laser power is plotted in logarithmic coordinates. A slope of ≈ 0.83 extracted from fitting of the experimental data of the WS_2/Si_3N_4/Ag is less than 1. This sublinear dependence indicates PL quenching in the WS_2/Si_3N_4/Ag at high laser powers, which is attributed to thermal accumulation caused by the low thermal conductivity of WS_2 monolayer [46]. Remarkably, a slope derived for nanocavity B at low laser powers is ≈ 1.37, exceeding unity. It arises from the proximity between the exciton resonance and MD resonance (≈ 630 nm), where the Purcell effect effectively enhances the PL intensity. In contrast, the

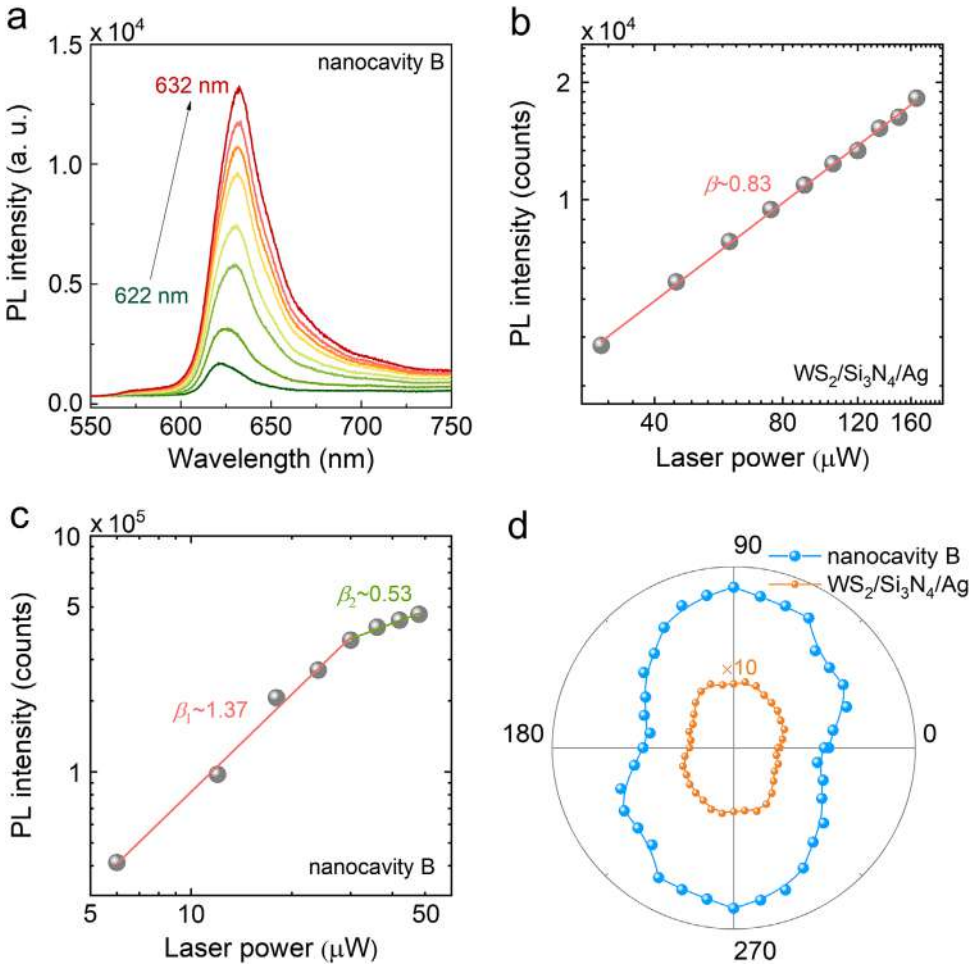

FIGURE 4 | Power-dependent PL intensity of a Si/WS_2/Si_3N_4/Ag nanocavity. (a) PL spectra measured for nanocavity B with fs laser power increasing from 6 to 48 μW. Dependences of the integrated PL intensity on the laser power observed for WS_2/Si_3N_4/Ag planar structure (b) and nanocavity B (c), respectively. (d) Dependences of the PL intensity on the polarization angle of the polarization analyzer measured for nanocavity B and the WS_2/Si_3N_4/Ag planar structure under the excitation of a 515 nm fs laser.

reduced slope (≈ 0.53) at high laser powers originates from the detuning of the exciton resonance from the MD resonance and PL quenching induced by the temperature rise. Therefore, PL intensity of the Si/WS_2/Si_3N_4/Ag nanocavity can be dynamically manipulated by adjusting the fs laser power. In order to examine the polarization of the PL emission from the Si/WS_2/Si_3N_4/Ag nanocavity and the WS_2/Si_3N_4/Ag planar structure, a polarization analyzer was placed in the signal collection channel. Figure 4d shows the dependence of the PL intensity on the polarization angle, confirming the linearly polarized nature of the emission.

2.5 | Enhanced PL Intensity from Si/WS_2/Si_3N_4/Ag Nanocavities Induced by Other Double Resonances

As the diameter of the Si nanoparticles increases, the ED resonance redshifts toward the exciton resonance, thereby enhancing the exciton emission owing to the enhanced electric field induced by the ED (see the white dashed line in Figure 1d). Figure 5a presents the multipolar decomposition for the resonances supported by a Si/WS_2/Si_3N_4/Ag nanocavity excited by a normally incident plane wave. It reveals that the resonant modes are dominated by the ED and MD resonances. Specifically, the ED resonance exhibits two peaks: one at ≈ 624 nm (long-wavelength) and the other at ≈ 474 nm (short-wavelength). Therefore, the electric field intensity induced by the ED resonance at the short-wavelength determines the 1PA in the WS_2 monolayer and 2PA in the Si nanoparticle. In Figure 5b, we examined electric field distributions $|E_{xy}|/|E_0|$ in the XY plane and $|E|/|E_0|$ in the XZ plane for a nanocavity at the ED resonance (short-wavelength). The electric field enhancements observed here are weaker than those induced by the ED resonance at the long-wavelength (see Figure 3a). Thus, the 2PA in the Si nanoparticle and the 1PA in the WS_2 monolayer are relatively weak under the resonant excitation at the short-wavelength ED resonance. In Figure 5c, we present the backward scattering spectra measured for four different Si/WS_2/Si_3N_4/Ag nanocavities with large diameters. One can observe that the long-wavelength ED resonance redshifts and approaches the exciton resonance. Moreover, the magnetic quadrupole (MQ) resonance gradually emerges in larger nanocavities. Note that the simulated MQ resonance in Figure 5a appears less pronounced under the normal incidence condition, in contrast to the oblique incidence condition employed in the experiment (see also Note S1) [34]. The scattering light shown in the CCD images features a white central spot surrounded by red and blue light. Figure 5d

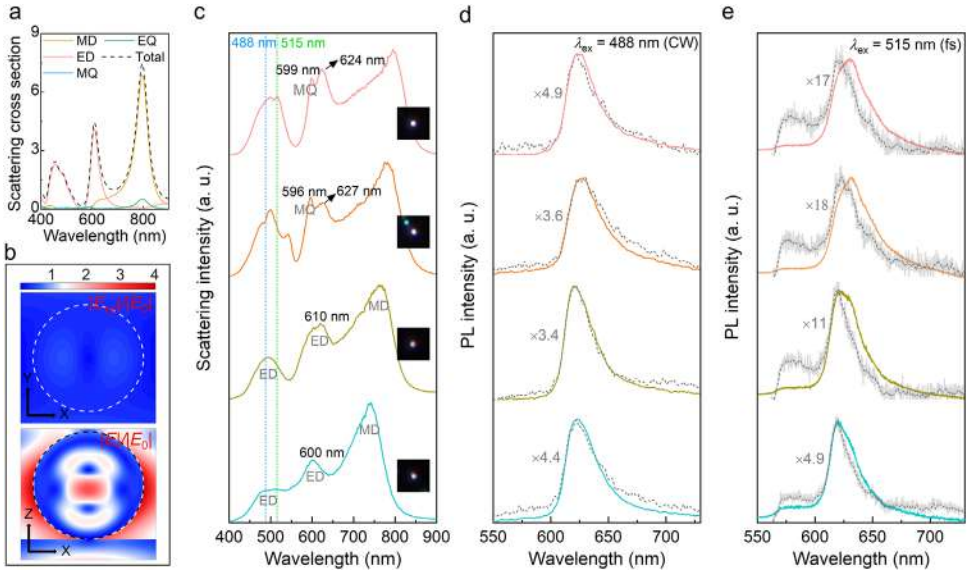

FIGURE 5 | Enhanced PL intensity from Si/WS_2/Si_3N_4/Ag nanocavities induced by other double resonances. (a) Multipolar decomposition of resonances for the Si/Si_3N_4/Ag nanocavity (d = 204.2 nm). The dashed curve indicates the sum of the scattering cross sections of the four multipolar components. (b) In-plane electric field distribution ($|E_{xy}|/|E_0|$) within the WS_2 monolayer in the XY plane and electric field distribution ($|E|/|E_0|$) in the XZ plane, calculated for a Si/WS_2/Si_3N_4/Ag nanocavity with d = 204.2 nm at the short-wavelength ED resonance (456 nm). (c) Backward scattering spectra measured for four Si/WS_2/Si_3N_4/Ag nanocavities. The CCD images of the corresponding scattering light are shown in the insets. PL spectra measured for the same four nanocavities (colored solid curves) and WS_2/Si_3N_4/Ag planar structures (gray dashed curves) under the excitation of a 488 nm CW laser (d) and a 515 nm fs laser (e), respectively.

presents the PL spectra measured for these four Si/WS_2/Si_3N_4/Ag nanocavities under the excitation of the 488 nm CW laser. It should be noticed that the excitation wavelength (488 nm) is resonant with the ED resonance (short-wavelength), resulting in an enhancement of the 1PA in the WS_2 monolayer. In each case, the PL spectrum measured for the adjacent WS_2/Si_3N_4/Ag planar structures is also provided for reference. In contrast to the pronounced redshifts observed in Figure 2d, the PL peaks of the nanocavities in Figure 5d exhibit negligible shifts. This is primarily because the energy of the lower plexciton formed by the coupling between the ED resonance and the exciton remains relatively high (see also Note S5). Moreover, the larger area of the hot spot induced by the ED resonance results in the dominant contribution to PL emission from uncoupled excitons (see also Note S3), which further explains the negligible redshift. Furthermore, although these nanocavities show enhanced PL intensity, their maximum relative PL intensity of ≈ 3.9 is lower than the corresponding value (≈ 5.6) observed in Figure 2d. This reduction is attributed to two factors: first, the 1PA in the WS_2 monolayer induced by the short-wavelength ED resonance is weaker than that induced by the long-wavelength ED resonance; second, the backward radiation intensity driven by the long-wavelength ED resonance is significantly weaker than that driven by the MD resonance (see Figure 1e; Figure S4). As shown in Figure 5e, we also present the PL spectra measured for these four nanocavities under the excitation of the 515 nm fs laser. The excitation wavelength (515 nm) is also close to the short-wavelength ED resonance, leading to the enhanced 1PA/2PA. A more pronounced redshift (≈ 9 nm) is observed under the fs laser excitation, compared to that under the CW laser excitation (see also Note S5). Moreover, one can also observe a significant enhancement in the PL intensity of the nanocavities. With the redshift of the ED resonance and the emergence of the MQ resonance, the relative PL intensity is enhanced via the Purcell effect. In addition, the maximum relative PL intensity reaches ≈ 17, which is far larger than that under the CW laser excitation (see Figure 5d). Nevertheless, this intensity is lower than that observed in Figure 2e due to the reduced backward radiation intensity and weakened 2PA/1PA processes. Therefore, a significant PL enhancement of the Si/WS_2/Si_3N_4/Ag nanocavity can also be realized via the enhanced 2PA/1PA and emission rate enhancement mediated by the ED resonance under the fs laser excitation.

Limited by the nanoscale region of electron transfer between the Si nanoparticle and the WS_2 monolayer and the fs timescale of this process, the direct observation of this process remains highly challenging. As previously reported [47], time-resolved pump–probe spectroscopy has been successfully employed to probe interlayer charge transfer (≈ 50 fs) in a MoS_2/WS_2 heterostructure without requiring high spatial resolution. Recently, it has been reported that the hot electron transfer between a Au nanoparticle and a $MoSe_2$ monolayer occurs on a timescale of ≈ 50 fs, which was characterized using time-resolved photoemission electron microscopy (TR-PEEM) due to its ultrahigh spatial and temporal resolution [23]. However, the fs laser used in this work has a pulse width of ≈ 130 fs, which is insufficient to resolve the ultrafast electron transfer process (≈ 50 fs). In subsequent work, we will collaborate to perform in situ observation of the electron transfer dynamics at the interface between a Si nanoparticle and a WS_2 monolayer using similar equipment, such as TR-PEEM. In addition, this work has successfully achieved significant PL enhancement based on a composite nanocavity. In future studies, the design of Si nanopillars or nanodisks could be further validated to replace the Si nanoparticles, thereby increasing the interaction area between the Si structures and the embedded

WS_2 monolayer. Such structural modifications are expected to substantially enlarge the charge-transfer interface, leading to stronger PL enhancement and further improving the potential for applications in photonic devices and high-efficiency light sources.

3 | Conclusions

In summary, we have systematically investigated the physical mechanism underlying the PL enhancement of a WS_2 monolayer embedded in a $Si/Si_3N_4/Ag$ nanocavity. Our findings reveal that the significantly enhanced 2PA in a Si nanoparticle under resonant fs laser excitation enables efficient electron transfer from the Si nanoparticle to the WS_2 monolayer, thereby boosting the PL emission of the latter. Our results demonstrate that the PL enhancement in $Si/WS_2/Si_3N_4/Ag$ nanocavities upon the fs laser excitation is approximately one order of magnitude higher than that upon the CW laser excitation. Moreover, weak coupling between the exciton and MD resonance further boosts the PL intensity, giving rise to the pronounced redshift observed in the PL spectra. Furthermore, additional enhancement in the PL intensity can be achieved through different double resonances, simultaneously enhancing excitation rate, emission intensity and emission directionality. In addition, we successfully manipulated the PL intensity of the nanocavity by tuning the laser power. Consequently, a significant PL *EF* of ≈ 13729 is achieved in the nanocavity at low laser power. The giant PL enhancement in the $Si/WS_2/Si_3N_4/Ag$ nanocavity demonstrated in this work suggests its potential application in nanoscale light-emitting devices.

4 | Experimental Section

4.1 | Sample Preparation

First, a 50 nm-thick Ag film was deposited on a SiO_2 substrate by using electron beam evaporation, followed by the deposition of a 90 nm-thick Si_3N_4 layer via high-frequency plasma-enhanced chemical vapor deposition (HF-PECVD) to form a Si_3N_4/Ag heterostructure. WS_2 monolayers grown on a Si substrate via CVD were then transferred onto the Si_3N_4/Ag heterostructure to create a $WS_2/Si_3N_4/Ag$ planar structure. Spherical Si nanoparticles with various diameters were fabricated by using fs laser ablation. The Si wafer immersed in deionized water was ablated by using 800-nm fs laser pulses (Legend Elite, Coherent) with a duration of 100 fs and a repetition rate of 1 kHz. Finally, an aqueous solution of Si nanoparticles was dropped on the $WS_2/Si_3N_4/Ag$ and dried naturally, obtaining $Si/WS_2/Si_3N_4/Ag$ nanocavities with tunable resonance wavelengths.

4.2 | Optical Characterization

The backward scattering spectra of $Si/WS_2/Si_3N_4/Ag$ nanocavities were measured by using a commercial optical microscope (BX51, Olympus) equipped with a standard dark-field illumination module. Scattered light was collected by a 50× objective (NA = 0.5), which was subsequently directed to a spectrometer (QE Pro High Performance, Ocean Insight) and a color CCD camera (Retiga R6, Teledyne Photometrics). For the PL measurements, two different excitation sources were employed. First, a 488 nm CW laser was introduced into the microscope and focused on the $Si/WS_2/Si_3N_4/Ag$ nanocavities or $WS_2/Si_3N_4/Ag$ planar structure by a 100× objective (NA = 0.9). Second, the PL measurements of the $Si/WS_2/Si_3N_4/Ag$ nanocavities were performed by using a fs laser oscillator (Mira-HP, Coherent) and an optical parametric oscillator (Mira OPO-X, Coherent) with a pulse duration of 130 fs and repetition rate of 76 MHz. The fs laser was introduced into an inverted microscope (Axio Observer A1, Zeiss) and focused on the nanocavities by using a 100× objective (NA = 1.3), which was subsequently directed to a spectrometer (SR-500i-B1, Andor) and a color CCD camera (DS-Ri2, Nikon).

4.3 | Numerical Simulations

The numerical simulations in this work were performed by using the finite-difference time-domain (FDTD) technique. The dielectric functions of Ag and Si were taken from Johnson and Christy [48] and from Palik [49], respectively, while that of the WS_2 monolayer was taken from the literature [8]. The refractive index of the surrounding medium was set to 1.0. In the calculation, the thickness of the WS_2 monolayer was set to 1.0 nm. A mesh size as small as 0.5 nm was used in the gap region between the Si nanoparticle and the WS_2 monolayer to ensure computational accuracy. Three-dimensional radiation patterns were simulated by employing a dipole source (615 nm) polarized along the x direction within a simulation size of 3.8 μm. In addition, the electromagnetic field distributions of resonant modes in the $Si/WS_2/Si_3N_4/Ag$ nanocavity were calculated by using plane waves. The scattering cross sections corresponding to the multipolar moments were then calculated based on the formulas described in the reference [50].

Acknowledgements

This work was financially supported by the National Natural Science Foundation of China (Grant Nos. 12374347, 12504442), the Guangdong Basic and Applied Basic Research Foundation (Grant Nos. 2025A1515012291, 2026A1515012069) and the Guangdong Provincial Department of Education Innovation Team Project (2024KCXTD043).

Conflicts of Interest

The authors declare no conflicts of interest.

Data Availability Statement

The data that support the findings of this study are available on request from the corresponding author. The data are not publicly available due to privacy or ethical restrictions.

References

1. B. Radisavljevic, A. Radenovic, J. Brivio, V. Giacometti, and A. Kis, "Single-Layer MoS_2 Transistors," *Nature Nanotechnology* 6 (2011): 147–150.

2. K. F. Mak and J. Shan, "Photonics and Optoelectronics of 2D Semiconductor Transition Metal Dichalcogenides," *Nature Photonics* 10 (2016): 216–226.

3. M. E. Kleemann, R. Chikkaraddy, E. M. Alexeev, et al., "Strong-Coupling of WSe_2 in Ultra-Compact Plasmonic Nanocavities at Room Temperature," *Nature Communications* 8 (2017): 1296.

4. K. F. Mak, C. Lee, J. Hone, J. Shan, and T. F. Heinz, "New Direct-Gap Semiconductor," *Physical Review Letters* 105 (2010): 136805.

5. A. Splendiani, L. Sun, Y. Zhang, et al., "Emerging Photoluminescence in Monolayer MoS_2," *Nano Letters* 10 (2010): 1271–1275.

6. Q. H. Wang, K. Kalantar-Zadeh, A. Kis, J. N. Coleman, and M. S. Strano, "Electronics and Optoelectronics of Two-Dimensional Transition Metal Dichalcogenides," *Nature Nanotechnology* 7 (2012): 699–712.

7. B. Zhu, X. Chen, and X. Cui, "Exciton Binding Energy of Monolayer WS_2," *Science Reports* 5 (2015): 9218.

8. Y. Li, A. Chernikov, X. Zhang, et al., "Measurement of the Optical Dielectric Function of Monolayer Transition-Metal Dichalcogenides: MoS_2, $MoSe_2$, WS_2, and WSe_2," *Physical Review B* 90 (2014): 205422.

9. L. N. Tripathi, O. Iff, S. Betzold, et al., "Spontaneous Emission Enhancement in Strain-Induced WSe_2 Monolayer-Based Quantum Light Sources on Metallic Surfaces," *ACS Photonics* 5 (2018): 1919–1926.

10. X. Zhou, Z. Zhang, and W. Guo, "Dislocations as Single Photon Sources in Two-Dimensional Semiconductors," *Nano Letters* 20 (2020): 4136–4143.

11. A. Carbone, D.-P. Bendixen-Fernex de Mongex, A. V. Krasheninnikov, et al., "Creation and Microscopic Origins of Single-Photon Emitters in Transition-Metal Dichalcogenides and Hexagonal Boron Nitride," *Applied Physics Reviews* 12 (2025): 031333.

12. H. Li, A. W. Contryman, X. Qian, et al., "Optoelectronic Crystal of Artificial Atoms in Strain-Textured Molybdenum Disulphide," *Nature Communications* 6 (2015): 7381.

13. A. Kayal, S. Dey, G. Harikrishnan, R. Nadarajan, S. Chattopadhyay, and J. Mitra, "Mobility Enhancement in CVD-Grown Monolayer MoS_2 via Patterned Substrate-Induced Nonuniform Straining," *Nano Letters* 23 (2023): 6629–6636.

14. S. Liu, Z. Lin, Y. Mao, et al., "Giant Enhancement of Second Harmonic Generation From WS_2 Monolayer Driven by Nanocavity-Induced Strain," *Laser & Photonics Reviews* 19 (2025): 00468.

15. S. Mouri, Y. Miyauchi, and K. Matsuda, "Tunable Photoluminescence of Monolayer MoS_2 via Chemical Doping," *Nano Letters* 13 (2013): 5944–5948.

16. Y. X. Lin, X. Ling, L. L. Yu, et al., "Dielectric Screening of Excitons and Trions in Single-Layer MoS_2," *Nano Letters* 14 (2014): 5569–5576.

17. J. Kern, A. Trügler, I. Niehues, et al., "Nanoantenna-Enhanced Light-Matter Interaction in Atomically Thin WS2," *ACS Photonics* 2 (2015): 1260.

18. J. Sun, H. Hu, D. Zheng, et al., "Light-Emitting Plexciton: Exploiting Plasmon–Exciton Interaction in the Intermediate Coupling Regime," *ACS Nano* 12 (2018): 10393–10402.

19. S. Park, N. Mutz, S. A. Kovalenko, et al., "Type-I Energy Level Alignment at the PTCDA—Monolayer MoS_2 Interface Promotes Resonance Energy Transfer and Luminescence Enhancement," *Advanced Science* 8 (2021): 2100215.

20. A. Karmakar, A. Al-Mahboob, C. E. Petoukhoff, et al., "Dominating Interlayer Resonant Energy Transfer in Type-II 2D Heterostructure," *ACS Nano* 16 (2022): 3861–3869.

21. M. Dandu, R. Biswas, S. Das, et al., "Strong Single- and Two-Photon Luminescence Enhancement by Nonradiative Energy Transfer across Layered Heterostructure," *ACS Nano* 13 (2019): 4795–4803.

22. D. Kozawa, A. Carvalho, I. Verzhbitskiy, et al., "Evidence for Fast Interlayer Energy Transfer in $MoSe_2/WS_2$ Heterostructures," *Nano Letters* 16 (2016): 4087–4093.

23. J. Tang, Y. Li, S. Ye, et al., "Direct Hot-Electron Transfer at the Au Nanoparticle/Monolayer Transition-Metal Dichalcogenide Interface Observed with Ultrahigh Spatiotemporal Resolution," *Nano Letters* 24 (2024): 2931–2938.

24. M. G. Harats, J. N. Kirchhof, M. Qiao, K. Greben, and K. I. Bolotin, "Dynamics and Efficient Conversion of Excitons to Trions in Non-Uniformly Strained Monolayer WS_2," *Nature Photonics* 14 (2020): 324–329.

25. Y. Jiang, H. Wang, S. Wen, H. Chen, and S. Deng, "Resonance Coupling in an Individual Gold Nanorod–Monolayer WS_2 Heterostructure: Photoluminescence Enhancement with Spectral Broadening," *ACS Nano* 14 (2020): 13841–13851.

26. C. Li, H. Luo, L. Hou, et al., "Giant Photoluminescence Enhancement of Monolayer WSe_2 Using a Plasmonic Nanocavity with on-Demand Resonance," *Nano Letters* 24 (2024): 5879–5885.

27. Y. H. Fu, A. I. Kuznetsov, A. E. Miroshnichenko, Y. F. Yu, and B. Luk'yanchuk, "Directional Visible Light Scattering by Silicon Nanoparticles," *Nature Communications* 4 (2013): 1527.

28. R. Yao, H. Sugimoto, T. Feng, et al., "Achieving Ideal Magnetic Light Emission with Electric-Type Emitters," *Nano Letters* 24 (2024): 13315–13323.

29. Y. Mao, S. Bai, M. Panmai, et al., "Controllable Shaping of High-Index Dielectric Nanoparticles by Exploiting the Giant Optical Force of Femtosecond Laser Pulses," *Photonics Research* 12 (2024): 282.

30. P. Ghenuche, S. Cherukulappurath, T. H. Taminiau, N. F. van Hulst, and R. Quidant, "Spectroscopic Mode Mapping of Resonant Plasmon Nanoantennas," *Physical Review Letters* 101 (2008): 116805.

31. C. Y. Zhang, Y. Xu, J. Liu, et al., "Lighting up Silicon Nanoparticles with Mie Resonances," *Nature Communications* 9 (2018): 2964.

32. J. H. Xu, Y. Wu, P. Z. Zhang, et al., "Resonant Scattering Manipulation of Dielectric Nanoparticles," *Advanced Optical Materials* 9 (2021): 2100112.

33. J. Xiang, J. D. Chen, Q. F. Dai, S. L. Tie, S. Lan, and A. E. Miroshnichenko, "Modifying Mie Resonances and Carrier Dynamics of Silicon Nanoparticles by Dense Electron-Hole Plasmas," *Physical Review Applied* 13 (2020): 014003.

34. T. Peng, Z. Wang, S. Li, et al., "Platform for Enhancing Light-Matter Interaction," *Photonics Research* 13 (2025): 709.

35. S. Liu, S. Li, Y. Mao, et al., "Manipulating the Exciton Dynamics in a MoS_2/WS_2 Heterobilayer with a Si/Au Nanocavity," *Laser & Photonics Reviews* 18 (2024): 2300850.

36. M. Ringler, A. Schwemer, M. Wunderlich, et al., "Shaping Emission Spectra of Fluorescent Molecules with Single Plasmonic Nanoresonators," *Physical Review Letters* 100 (2008): 203002.

37. J. Cambiasso, M. König, E. Cortés, S. Schlücker, and S. A. Maier, "Surface-Enhanced Spectroscopies of a Molecular Monolayer in an All-Dielectric Nanoantenna," *ACS Photonics* 5 (2018): 1546–1557.

38. H. Shinomiya, H. Sugimoto, T. Hinamoto, Y. J. Lee, M. L. Brongersma, and M. Fujii, "Enhanced Light Emission from Monolayer MoS_2 by Doubly Resonant Spherical Si Nanoantennas," *ACS Photonics* 9 (2022): 1741–1747.

39. J. Fang, M. Wang, K. Yao, et al., "Directional Modulation of Exciton Emission Using Single Dielectric Nanospheres," *Advanced Materials* 33 (2021): 2007236.

40. A. F. Cihan, A. G. Curto, S. Raza, P. G. Kik, and M. L. Brongersma, "Silicon Mie Resonators for Highly Directional Light Emission from Monolayer MoS_2," *Nature Photonics* 12 (2018): 284–290.

41. K. Ozawa, H. Sugimoto, D. Shima, et al., "Routing Light Emission from Monolayer MoS_2 by Mie Resonances of Crystalline Silicon Nanospheres," *ACS Applied Optical Materials* 3 (2025): 375–382.

42. M. Aagaard, S. P. S. Jessen, J. L. Hansen, R. M. Turtos, P. Balling, and B. Julsgaard, "Two- and Three-Photon Absorption in Silicon for above-Band-Gap Photon Energies," *Physical Review B* 112 (2025): 155210.

43. A. Krasnok, S. Glybovski, M. Petrov, et al., "Demonstration of the Enhanced Purcell Factor in all-Dielectric Structures," *Applied Physics Letters* 108 (2016): 211105.

44. D. G. Baranov, R. S. Savelev, S. V. Li, A. E. Krasnok, and A. Alù, "Modifying Magnetic Dipole Spontaneous Emission with Nanophotonic Structures," *Laser & Photonics Reviews* 11 (2017): 1600268.

45. S. Liu, F. Deng, W. Zhuang, et al., "Optical Introduction and Manipulation of Plasmon–Exciton–Trion Coupling in a Si/WS_2 /Au Nanocavity," *ACS Nano* 16 (2022): 14390–14401.

46. L. Su, Y. Yu, L. Cao, and Y. Zhang, "Effects of Substrate Type and Material-Substrate Bonding on High-Temperature Behavior of Monolayer WS_2," *Nano Research* 8 (2015): 2686–2697.

47. X. Hong, J. Kim, S. F. Shi, et al., "Ultrafast Charge Transfer in Atomically Thin MoS_2/WS_2 Heterostructures," *Nature Nanotechnology* 9 (2014): 682–686.

48. P. B. Johnson and R. W. Christy, "Optical Constants of the Noble Metals," *Physical Review B* 6 (1972): 4370–4379.

49. F. Deng, H. Huang, J. D. Chen, et al., "Greatly Enhanced Plasmon–Exciton Coupling in Si/WS_2 /Au Nanocavities," *Nano Letters* 22 (2022): 220–228.

50. R. Alaee, C. Rockstuhl, and I. Fernandez-Corbaton, "An Electromagnetic Multipole Expansion beyond the Long-Wavelength Approximation," *Optics Communications* 407 (2018): 17–21.

Supporting Information

Additional supporting information can be found online in the Supporting Information section.

Supporting File: lpor71283-sup-0001-SuppMat.docx.